Volumetric Simulation of Nano-Fibres and 2D SEM and 3D XCT Imaging Processes

John P. Chiverton[1,3][0000−0001−9081−4136], Alexander Kao[2,3], Marta Roldo[4,5][0000−0003−2242−7761], and Gianluca Tozzi[2,3][0000−0002−3172−5720]

[1] School of Energy and Electronic Engineering,
[2] School of Mechanical and Design Engineering,
[3] Zeiss Global Centre,
[4] School of Pharmacy and Biomedical Sciences,
[5] Institute of Biomedical and Biomolecular Sciences,
University of Portsmouth, UK.
{john.chiverton,alexander.kao,marta.roldo,gianluca.tozzi}@port.ac.uk

Abstract. Fibres are present in many biological tissues and their geometric properties can be a useful indication of their role. Hence, imaging of nano-fibre volumes is useful for a number of different biomedical applications. It is possible to image nano-fibres with a variety of imaging modalities such as 2D Scanning Electron Microscopy (SEM) or 3D X-ray Computed Tomography (XCT). The 3D XCT has some advantages over conventional SEM. The principal ability is to gain an understanding of the 3D structure of objects. However, XCT has limited resolution compared to SEM. This means SEM can be useful to provide more detailed specific estimates of the sizes of structures such as estimates of the diameters of fibres. Image processing of these images has resulted in the need for a gold standard to help demonstrate the correct functioning and validation of designed algorithms. Simulation can play an important part in the validation of algorithms. However, previous works have performed limited simulations. Some methods simulate fibres as straight vectors. The approach taken here is more realistic, allowing for curving, overlapping and other more realistic generation of fibre volumes with the use of splines. The limited resolution in the imaging processes are also considered here, another important factor. Simulation results are compared with real world imaging data from both SEM and XCT. The generated results appear to show similar properties and could potentially be used as gold standards for the validation of image processing algorithms.

Keywords: Nano-Fibres · Volumetric Imaging · Simulation.

1 Introduction

Biomedical tissues contain a variety of structures. Fibres are commonly found in biomedical tissues and their characterisation can be an important consideration in various tasks. For instance, elastin and collagen fibres have different roles and are found through out the body such as in the articular cartilage e.g. [5] and

elsewhere such as in scar tissue [6]. Fibres can also be synthetically engineered for a number of roles such as acting as tissue scaffolds [8]. The geometry and other aspects related to the structure of the fibres can play an important role in these situations [9]. Imaging can therefore be very useful in characterising fibres and hence their biomedical functions.

Imaging of nano-fibres is possible with a number of different imaging modalities such as 2D based Scanning Electron Microscopy (SEM) or 3D X-ray Computed Tomography (XCT). The 3D XCT has some advantages over conventional 2D SEM, principally the ability to gain an understanding of the 3D structure of objects. However the resolution in 3D XCT is not as good as the resolution of 2D SEM. This means 2D SEM can be useful to provide more detailed specific estimates of 3D structures. The two sources of imaging information can however be combined to provide more detailed understanding of sizes of fibres in 3D. This was the approach taken in our previous work in [2], where electrospun poly(caprolactone) PCL nano-fibre samples were prepared and then imaged with SEM and XCT modalities.

A number of authors have sought to simulate nano-fibres for the purposes of acting as a gold standard for testing algorithms [1] and for gaining insights into a number of aspects. This has included estimating pore sizes in 2D by [3] and orientation distributions in [4]. Fibres were modelled as straight lines in 2D in these papers. It is possible to simulate fibres in 3D as in our previous work [1]. However a limitation in all these works is that the fibres are simulated as straight vectors, rather than something more realistic such as splines or similar.

Other authors have investigated the use of more advanced fibre models, such as to simulate the fibres in muscles [7]. Little detail was given except in terms of the presentation of the idea of using B-Splines to model the fibres.

A further disadvantage of these methodologies and others is that the imaging process is not taken into account. The limited resolution in 3D can limit the accurate estimation of various measures such as angles and pore sizes. This work therefore considers a more holistic fibre simulation process, in 3D, taking into account the limiting resolution in the imaging process.

2 Methodology

For this work, a simulation pipeline was devised to simulate the properties of electrospun nano-fibre mats. The simulation process is summarised in Fig. 1.

Initially N fibres are simulated in 2D, $\phi_s(t) = ((x_t, y_t)|0 \leq t \leq 1)$. They are modelled here as B-splines

$$(x_t, y_t)^{\mathrm{T}} = \sum_{l=0}^{n} P_l^2 B_{l,k}(t \times L) \tag{1}$$

where P_l^2 are 2D control points with $l = [0, n]$; $B_{l,k}$ are basis functions of order k, $t \in [0, 1]$ and L is defined so that the argument of the basis functions extends to

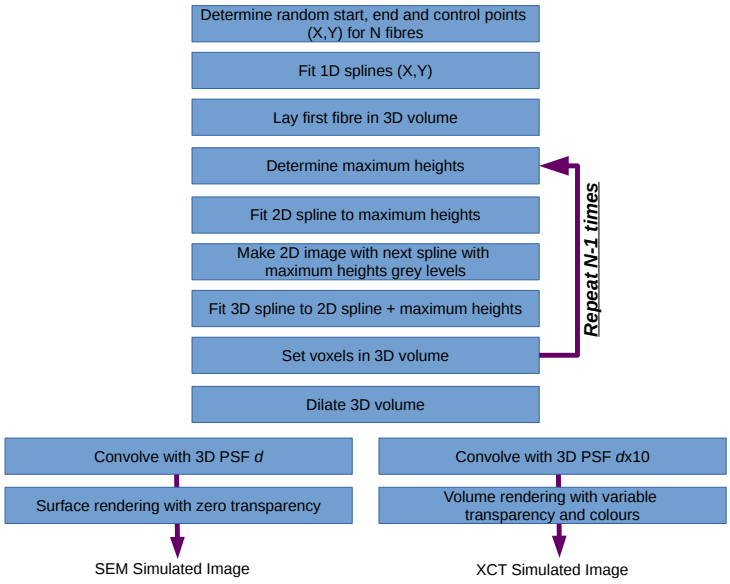

Fig. 1. Illustration of the processing pipeline used here to simulate the properties of electrospun nano-fibres mats.

the range over which the basis functions are defined. The control points are randomly sampled from a uniform distribution to vary randomly along overlapping channels in the 2D space.

The result of this *random* B-spline generation process can be considered purely in the form of a 2D Cartesian representation with

$$\Phi_i(x,y) = \begin{cases} \delta(x-u, y-v) & \text{where } (u,v) \in \phi_i(t), \\ 0 & \text{elsewhere;} \end{cases} \tag{2}$$

where $\delta(x-u, y-v)$ is the shifted Dirac delta which is infinitesimal thin but infinitely tall at $x = u$ and $y = v$. Also, taking $\int_{-\infty}^{\infty}\int_{-\infty}^{\infty} \delta(x,y)\mathrm{d}x\mathrm{d}y = 1$. Some examples of discrete approximations of $\sum_{i=0}^{N-1} \Phi_i(x,y)$ for different numbers of N are illustrated in Fig. 2.

An important aspect here is to extend this to 3D and to make sure that the fibres do not physically intersect. Thus, fibres are placed sequentially, starting from the bottom and then building up. If a fibre is located in a position that is directly above or crosses another fibre or fibres then the height of the newly laid fibre is modified at points depending on the positioning of those fibres. This is illustrated in Fig. 3.

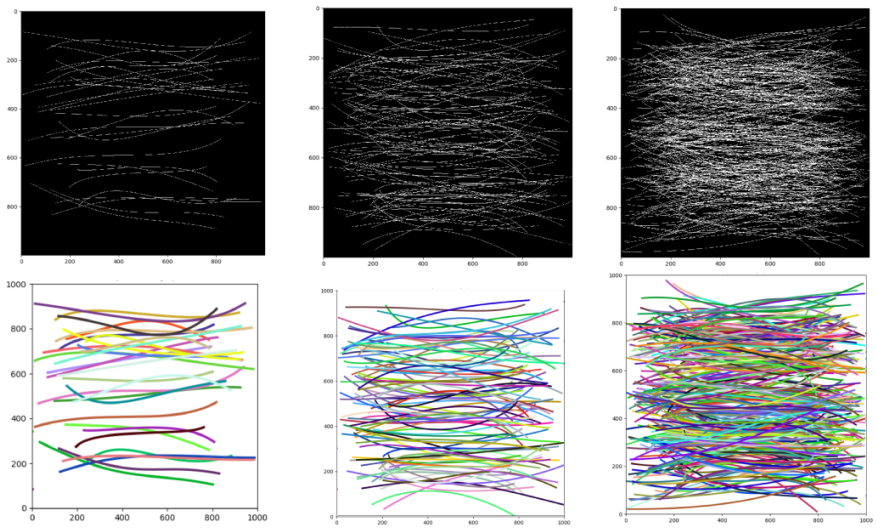

Fig. 2. Illustrations of varying numbers of b-splines with $N = 30$, 100 and 300. Top rows shows the centre lines of the fibres and the bottom row shows each fibre individually colour coded.

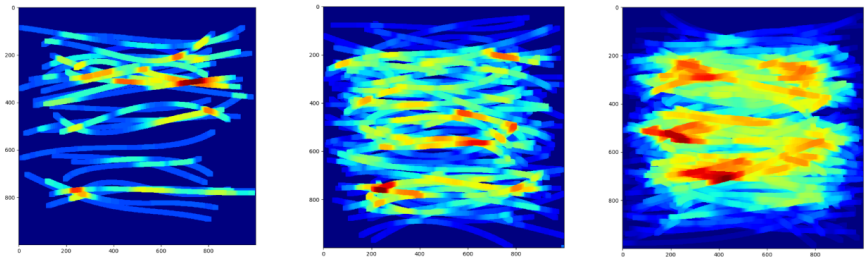

Fig. 3. Illustrations of the effect of the positioning of fibres on top of other fibres. Fibres at a greater height have a different colour value. From left to right with $N = 30$, 100 and 300.

The process of determining the points through which a fibre should be raised (i.e. interpolated) is based on a sum across all the currently placed fibres:

$$M_i(x,y) = \sum_{j=0}^{i-1} \Phi_j(x,y) \times \Delta_z \tag{3}$$

where $\Phi_j(x,y)$ is the 2D representation of the j^{th} laid fibre at pixel location x, y and Δ_z controls the vertical distancing and hence vertical positioning of the fibres. Then the i^{th} laid fibre can then be modelled in 3D with $\theta_i(t) = ((x_t, y_t, z_t)|z_t = M_i(x_t, y_t), 0 \leq t \leq 1)$. This process is illustrated in Fig. 4.

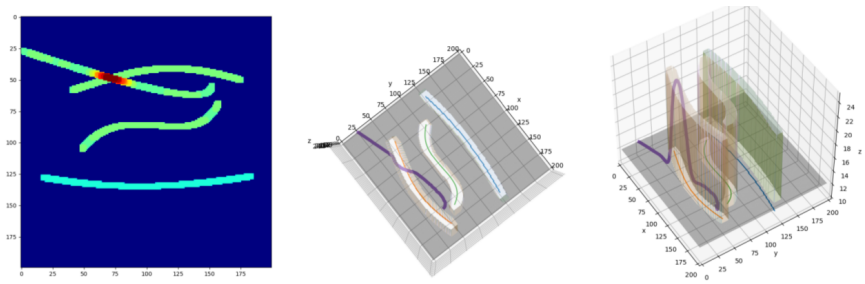

Fig. 4. Further illustrations of the effect of the positioning of fibres on top of other fibres for a single case of $N = 4$. Left shows four fibres with one overlapping another. This overlapping fibre is the last to be laid and is shown in the middle and right views in 3D being positioned above the underlying fibre.

The 3D fibres are also modelled here as B-splines so that $z_t \approx M_i(x_t, y_t)$ similar to (1) except extended to 3D with $(x_t, y_t, z_t)^{\text{T}} = \sum_{l=0}^{n} P_l^3 B_{l,k}(t \times L)$. They can then be considered in 3D with

$$\Theta_i(x,y,z) = \begin{cases} \delta(x-u, y-v, z-w) & \text{for } (x,y,z) \in \theta_i(t), \\ 0 & \text{elsewhere.} \end{cases} \tag{4}$$

The resulting volume consisting of N fibres can then be constructed as the sum of the individual volumes, i.e.

$$\Theta(x,y,z) = \sum_{i=0}^{N-1} \Theta_i(x,y,z). \tag{5}$$

The electrospun fibres have different intensity properties in these two imaging domains. A related aspect and difference between the SEM and XCT imaging modalities is the difference in the underlying image resolution. The sampling

process can be considered to involve convolution with a Point Spread Function (PSF), i.e.

$$\Theta(x,y,z) * G(x,y,z) = \int_{-\infty}^{\infty}\int_{-\infty}^{\infty}\int_{-\infty}^{\infty} \Theta(x-u,y-v,z-w)G(u,v,w)\mathrm{d}u\mathrm{d}v\mathrm{d}z. \quad (6)$$

Here, a stationary and symmetric Gaussian PSF is assumed for $G(x,y,z)$ for both SEM and XCT simulation:

$$G(x,y,z) = \frac{1}{(2\pi\sigma^2)^{D/2}} \exp\left(-\frac{x^2+y^2+z^2}{2\sigma^2}\right). \quad (7)$$

A wider PSF for the XCT is selected for the simulation of the XCT images. This means that the information is more blurred and the effective resolution is reduced.

3 Experiments and Results

3.1 Imaging

Previously, for our work in [2], Electrospun poly(caprolactone) (PCL) nanofibre samples were prepared. SEM images were obtained for gold-coated samples (sputter coater Q150R, Quorom Technologies) with a Zeiss EVO MA10 scanning electron microscope with electron back-scatter capability. A Zeiss Xradia Versa 520 Microtomography X-Ray Computer Tomography (XCT) system was also used for XCT image acquisition with an image voxel size of 0.15x0.15x0.15μm^3.

Exemplar SEM images can be seen in Fig. 5. Exemplar XCT images can be seen visualised using volume rendering in Fig. 6.

3.2 Simulation

A fibre volume consisting of $N = 700$ fibres was simulated. The volume consisted of $1000 \times 1000 \times 1000$ voxels. A discrete approximation $\Theta(x,y,z)$ was used, where each contributing $\delta(x,y,z)$ was replaced with a discrete unit impulse function. This yielded a 3D volume with fibres of finite width of at most 1 voxel, $\Theta'_N(\mathbf{x})$ where $\mathbf{x} = (x',y',z')$ are integer values. Morphological 3D dilations were then used to approximate fibres with somewhat greater diameters. A 3D almost cubic structuring element, B with dimensions $4 \times 4 \times 4$ was used, i.e. $\Theta'_N(\mathbf{x}) \oplus B$.

As described, 3D dilations were used to provide reasonable width fibres. Execution time took approximately 30 minutes on a workstation with a Xeon core processor and 64GB of RAM. Python eco-system was used together with scipy and scikit-image.

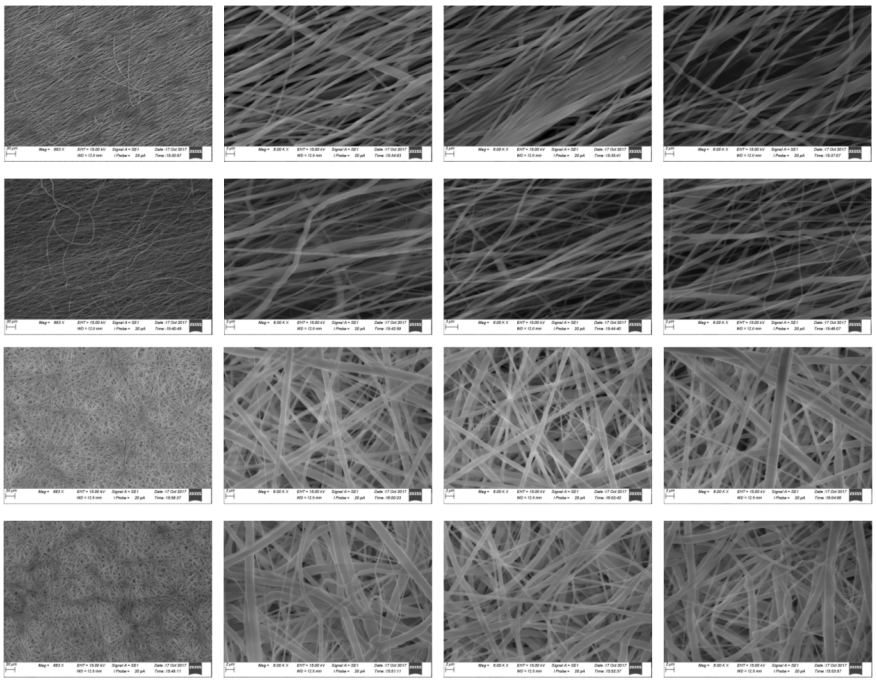

Fig. 5. SEM images of a fibre sample at two different resolutions for the two samples.

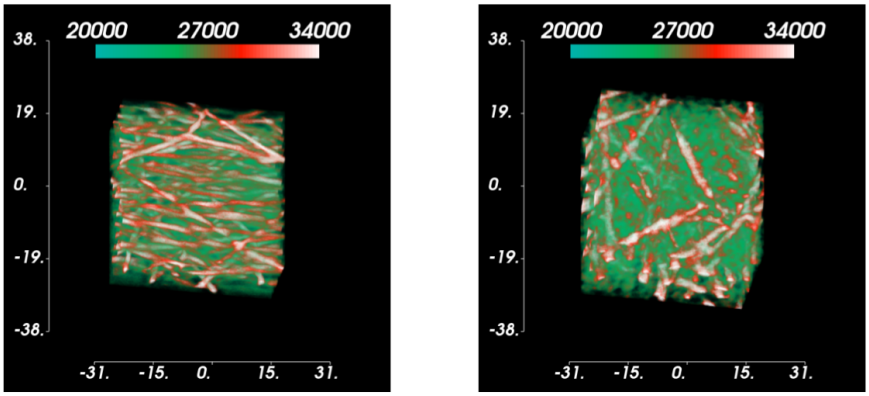

Fig. 6. 3D visualisation of sub-volumes or XCT regions of interests of a sample with (left) aligned fibres and (right) random fibres. Units are in mm.

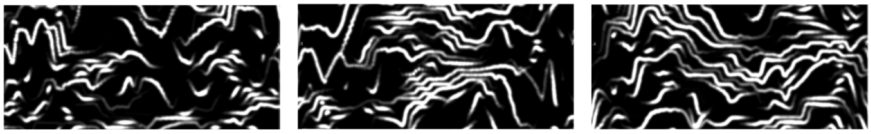

Fig. 7. Some exemplar cross sections through the volume. A PSF with $\sigma = 3$ was used here. These slices help to illustrate the way that fibres have been laid, appearing to show some success in the designed system process. However, there are limitations to what can be perceived in these 2D cross sections.

3.3 Fibre Laying Process

It is interesting to observe whether the fibres were laid in a way that is consistent with the overall goals of the simulation process. Therefore some exemplar cross-sectional slices are presented in Fig. 7.

The exemplar cross sections appear to show success in the designed approach in terms of ensuring fibres are not intersecting. It can also be observed that interaction of the fibres depends on the action of the PSF as well.

3.4 PSF Width Selection

A number of different width PSF were considered, initially for simulation of the SEM images. Some results can be seen in Fig. 8.

The different results represent a range of different scenarios. Some more successful than others. For instance, the result in the top left is demonstrating excessive beading. This is actually a possible scenario in the generation of synthetic fibres. However, it has less potential uses compared to fibres that have been generated in a more consistent fashion, where continuity is preserved. The two results in the top middle and top right are convolved with a greater width PSF. These results appear to be closer in similarity with the appearance of fibres in XCT based images. In contrast to those, the images in the bottom of Fig. 8 appear more consistent with SEM based acquired images, as shown in Fig. 5. However the bottom middle image is from the underside of the generated volume which appears to be less similar to the appearance of the actual data. This is partly due to it being the first layer in which the fibres are laid.

3.5 3D XCT Simulation

The above results can be considered potentially useful for a SEM like simulation result. The same data was also convolved with a wider PSF ($\sigma = 10$) to simulate the effective resolution for XCT. Down-sampling was also performed by a factor of 10 resulting in a volume of $100 \times 100 \times 100$ voxels. Results of volume rendering can be seen in Fig. 9.

The generated volume renderings appear to be somewhat similar to the volume renderings of the real data. Higher ranges in intensities result when there

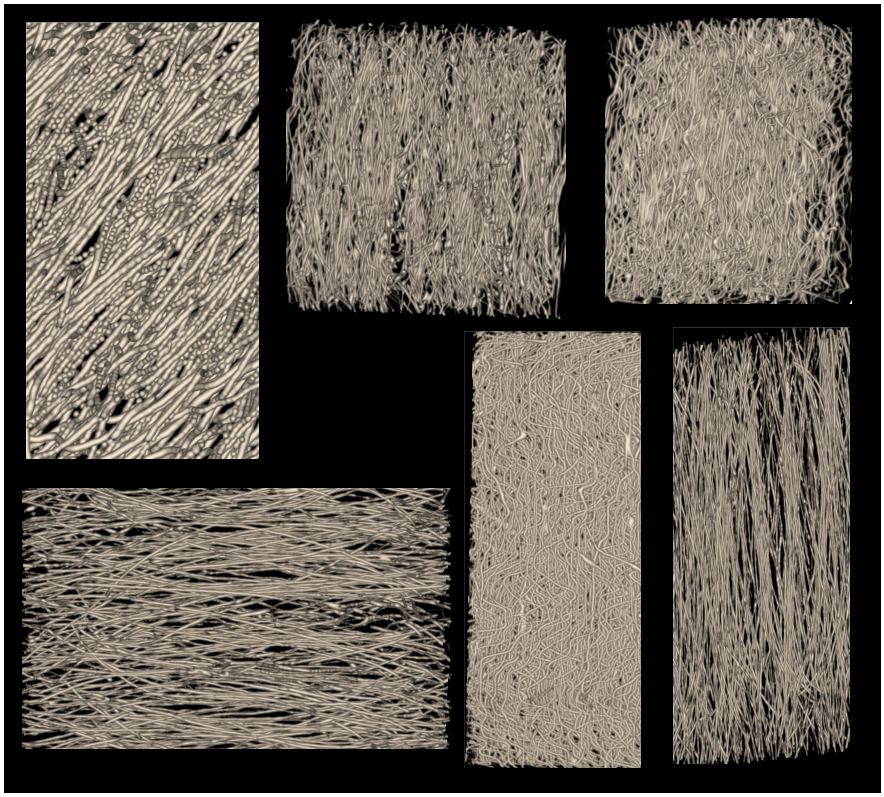

Fig. 8. Some surface rendering results for different PSFs for SEM simulation. Top left has $\sigma = 2$; top middle and right have $\sigma = 5$. Bottom have $\sigma = 3$. When the PSF is too narrow (i.e. $\sigma = 2$), then artefacts associated with the limited discrete approximation of the fibre geometries become apparent. If the PSF is too wide, then the fibres start to merge, which is more similar to what can be observed in XCT.

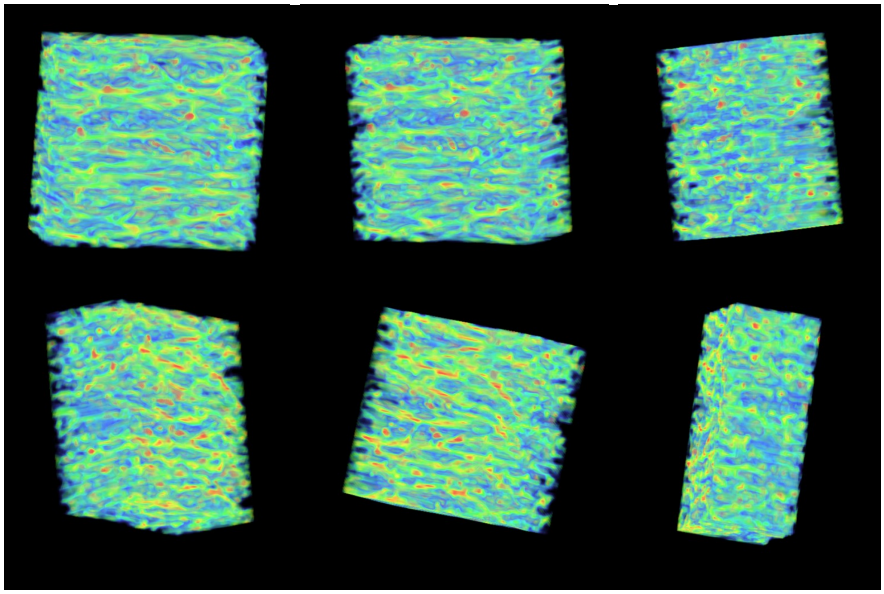

Fig. 9. Volume rendering after the simulation of the XCT imaging process.

are clusters of fibres in the same vicinity due to the action of the PSF in (6). This can be similarly observed for the volume renderings of the real data, as shown in Fig. 6.

4 Discussion and Conclusions

A fibre simulation process has been described. Some basic steps have also been performed to simulate the imaging processes for two modalities with different imaging resolutions, such as SEM and XCT. Results appear to show some interesting similarities with real imaging data. Future work will include investigations into potential applications of these simulations.

References

1. Chiverton, J.P., Ige, O., Barnett, S.J., Parry, T.: Multiscale shannons entropy modeling of orientation and distance in steel fiber micro-tomography data. IEEE Transactions on Image Processing **26**(11), 5284–5297 (2017)
2. Chiverton, J.P., Kao, A., Roldo, M., Tozzi, G.: Automatic diameter and orientation distribution determination of fibrous materials in micro x-ray ct imaging data. Journal of microscopy **272**(3), 180–195 (2018)
3. Danwanichakul, P., Danwanichakul, D.: Two-dimensional simulation of electrospun nanofibrous structures: connection of experimental and simulated results. Journal of Chemistry **2014** (2014)

4. Feng, Y., Sun, R., Chen, M., Liu, C., Wang, Q.: Simulation of the morphological structures of electrospun membranes. Journal of Applied Polymer Science **135**(1), 45653 (2018)
5. He, B., Wu, J., Chim, S.M., Xu, J., Kirk, T.B.: Microstructural analysis of collagen and elastin fibres in the kangaroo articular cartilage reveals a structural divergence depending on its local mechanical environment. Osteoarthritis and cartilage **21**(1), 237–245 (2013)
6. Mostaço-Guidolin, L., Rosin, N.L., Hackett, T.L.: Imaging collagen in scar tissue: developments in second harmonic generation microscopy for biomedical applications. International journal of molecular sciences **18**(8), 1772 (2017)
7. Ng-Thow-Hing, V., Agur, A., McKee, N.: A muscle model that captures external shape, internal fibre architecture, and permits simulation of active contraction with volume preservation. In: ISCM Biomechanics & Biomedical Eng. (5.: 2001: Rome) (2001)
8. Sensini, A., Gualandi, C., Focarete, M.L., Belcari, J., Zucchelli, A., Boyle, L., Reilly, G.C., Kao, A.P., Tozzi, G., Cristofolini, L.: Multiscale hierarchical bioresorbable scaffolds for the regeneration of tendons and ligaments. Biofabrication **11**(3), 035026 (2019)
9. Urszula, S., Szewczyk, P., Kruk, A., Barber, A., Czyrska-Filemonowicz, A.: 3D imaging via FIB-SEM tomography at nanoscale for tissue engineering applications. In: European Microscopy Congress 2016: Proceedings. pp. 318–319. Wiley Online Library (2016)